Size-dependence of the electronic properties of two-dimensional Cu–O clusters: new Monte Carlo trajectory algorithm

V. F. Elesin and V. A. Kashurnikov

Moscow Engineering Physics Institute, 115409 Moscow, Russia

A new Monte Carlo trajectory algorithm is proposed for calculating the electronic properties of two-dimensional Cu–O clusters. This algorithm is an extension of the one described previously by J. E. Hirsch *et al.* for the one-dimensional Hubbard model. The energy E, the occupation numbers $\langle N_{Cu} \rangle$ and $\langle N_O \rangle$ of the copper and oxygen orbitals, respectively, the optical gap in the one-particle spectrum Δ_{opt}, the spin correlation functions S_{ij}, and the momentum distribution functions $n(\mathbf{k})$ were calculated for a series of Cu–O clusters with $N_a = 12$, 24, 30, 48, 54, 60, 78, 96, 102, and 108 sites. The properties listed above were determined for the first time as a function of the dimensions of the system. Specifically, it was found that at some critical value of N_a the quantities E, $\langle N_{Cu} \rangle$, $\langle N_O \rangle$, and S_{ij} no longer depend on the cluster size. The antiferromagnetic correlation length was calculated and found to be three lattice periods (~ 1 nm) at $N_a = 54$; this agrees with the experimental value and is much less than the linear size of a cluster. It is shown that the character of the suppression of the antiferromagnetic correlations accompanying doping with electrons and holes, as observed previously in the cluster Cu_4O_8, is also maintained for large systems; this indicates that a "magnetic" mechanism of attraction operates between excess carriers in a CuO_2 plane. © *1994 American Institute of Physics.*

1. INTRODUCTION

The discovery of high-T_c superconductors has stimulated great interest in electronic systems with strong correlation effects. The most popular models are the Hubbard[1-3] and Emory[4] models. The latter model describes the CuO_2 plane—the basic structural element of these compounds. In spite of the large number of treatments (see, for example, Refs. 2, 3, 5, and 6) that have been carried out, Emory's model is not adequately understood and it is difficult to make analytical investigations within this model. As a result, numerical methods, such as the exact diagonalization method (EDM)[7-11] and the Monte Carlo method (MCM),[12-16] become important. These methods make it possible to calculate accurately the properties of the ground and excited states in finite systems. A distinguishing feature of the EDM is that the energy of the ground state (at $T=0$) and the correlation functions in small finite clusters (the number of atoms $N_a \sim 10$) can be calculated to any desired accuracy. The results obtained for Cu–O clusters with the EDM[5,7,10,17,18] have demonstrated that carriers can be attracted to one another as a result of antiferromagnetic correlations; this points to a magnetic mechanism of high-T_c superconductivity. The EDM can also be used to investigate the excited states of a system.[19,20] This makes it possible to determine the electronic properties, such as the density of one-particle states,[21-23] the dynamic conductivity,[24,25] and others.

The fundamental drawback of the EDM is that the size of the working memory and the speed of modern computers limit the cluster sizes, and this makes it impossible to investigate the effect of cluster sizes on the electronic and thermodynamic properties. This is especially clearly demonstrated in the case of the CuO_2 plane. Indeed, the maximum Cu–O cluster with the symmetry of the CuO_2 plane and allowing application of the EDM is Cu_4O_8.[10] The next square cluster has $N_a = 24$ atoms and can no longer be handled by the EDM (the Hamiltonian matrix contains more than 10^{16} elements, even for an undoped dielectric state of this cluster).

For this reason, quantum Monte Carlo methods must be used to investigate the effect of the cluster size on the properties of a system.[12-14] These methods make it possible to calculate the properties of large clusters ($N_a = 100-200$). The drawback of these methods is that it is impossible to investigate the most interesting range of low temperatures $T \sim 100$ K, since in this case the statistical errors grow rapidly and the computing time increases. Monte Carlo methods have been used to calculate the density of one-particle states,[26-28] the momentum distribution,[29-34] and the charge, spin, and pair correlation functions.[35-38] They have also been used to study the pairing symmetry[5,38] for one- and two-dimensional systems in the Hubbard, t-J, and Emory models with $N_a \sim 20-100$.

Variational Monte Carlo methods[39-41] based on minimizing an energy functional with different types of variational functions are distinguished from quantum, "thermal" Monte Carlo methods, which employ the Trotter expansion[42,43] and the Metropolis algorithm.[44] Variational Monte Carlo methods, which in many cases satisfactorily describe the ground state, are very sensitive to the initial approximation and the form of the model being investigated. The results are strongly affected by the choice of the variational function.[39,40] In this sense, quantum Monte Carlo methods are more universal. They are divided into so-called determinant algorithms,[22,45] extended to interacting systems[46,47] by means of the discrete Hubbard–Stratonovich transformation proposed by J. E. Hirsch,[48] and trajectory

methods.[12,13,49,50] In these algorithms the d-dimensional quantum problem reduces to a $(d+L)$-dimensional classical problem; in addition, $L=1$ for trajectory Mont Carlo methods and $L \geq 1$ for determinant methods.

We note that trajectory algorithms are much more efficient and converge more rapidly than determinant algorithms, but they have been developed mainly for one-dimensional fermion systems. (However, these algorithms are used successfully for two-dimensional Heisenberg antiferromagnets[51] and for one-dimensional[50,52,53] and two-dimensional[54] systems with boson degrees of freedom.) The efficiency of these methods is based on the fact that the calculation employs a canonical ensemble with a fixed number of particles. This reduces considerably the size of the Hilbert space of the possible site states. As the number N_a of sites in the system increases, the number of Monte Carlo steps required increases as N_a, while the number of steps increases as $\sim N_a^3$ in the case of determinant Monte Carlo methods.[46]

Determinant Monte Carlo methods have been used successfully to study both one- and two-dimensional systems.[36,55,56] These methods are based on a transformation of the statistics of the fermion degrees of freedom to Ising-spin-type statistics. This simplifies the Monte Carlo procedure and makes it possible to circumvent questions concerning the dimension of the system.[46] This transformation must be paid for by working with the grand canonical ensemble with a variable number of particles and a considerably slower rate of convergence than in the case of trajectory methods. In the Monte Carlo procedure the Green's function is calculated directly.[36,47] This simplifies the subsequent calculations of the correlation functions[35] and makes it possible to calculate the band structure[26–28] and the momentum distribution.[29,30] One drawback of determinant Monte Carlo methods as compared to the trajectory algorithm is that the number of spin variables over which the Monte Carlo procedure is performed increases (i.e., the dimension of the corresponding classical problem increases) as the number of bands in the model under study increases, since under a discrete Hubbard–Stratonovich transformation each pair interaction results in the appearance of a new spin variable.[46,48]

Determinant algorithms also come in several modifications. For example, M. Imada et al.[36] proposed a combination of the standard "thermal" Monte Carlo method and Gram–Schmidt reorthogonalization at low temperatures; this makes it possible to investigate states with lower energy. A combination of the standard Monte Carlo process and molecular dynamics is considered in Ref. 38. S. Sorella[57] proposed a modified Monte Carlo procedure for analyzing the ground state of a fermion system by means of special projection operators. This made it possible to investigate the distribution function $n(\mathbf{k})$[30,32] and show that there is no Fermi discontinuity for a one-dimensional one-band Hubbard model.

We recall here one other problem that complicates the Monte Carlo procedure: the minus sign problem. This problem arises for two- and three-dimensional fermion systems.[58] It arises as a result of the antisymmetry of the fermion wave function. This results in the appearance of a negative sign in the statistical weight of different Monte Carlo configurations and it increases the statistical errors and the computational time. In Ref. 58 different methods are proposed for solving this problem, depending on whether or not the average sign of a configuration approaches zero or a constant in the limit $T \rightarrow 0$.

We now discuss in greater detail the trajectory Monte Carlo algorithms.[12,15,59,60] First developed by J. E. Hirsch et al.,[12–14] these algorithms are employed exclusively for one-dimensional fermion systems. The main idea of the algorithm is to transform the d-dimensional quantum problem to a $(d+1)$-dimensional classical problem by introducing "time" slices on the imaginary time axis $0 < \tau < \beta = 1/T$ and to implement the Monte Carlo procedure in the space imaginary time τ—coordinate L. The transformation from the one- to the two-dimensional (in real space) problem is in principle possible (as noted in Ref. 13), and it has been used for boson degrees of freedom,[50–54] but it involves the above-mentioned sign problem and can result in large statistical errors and greater computing time. It is this difficulty that has prevented applications of this algorithm to two-dimensional fermion systems.

Trajectory algorithms are less sensitive to the multiband nature of the models considered than are determinant algorithms, since in the latter case the dimension of the corresponding classical problem increases with the number of bands and is obviously $\geq d+1$, while for trajectory Monte Carlo methods it always equals $d+1$. It is very important that the calculations are performed with a fixed number of particles (and when spin is present, the projection of the total spin $\langle S_z \rangle$ is also fixed). This is convenient for both efficient convergence and analysis of the density dependence.

Summarizing the analysis of Monte Carlo algorithms, we note that because of the great difficulties of using standard Monte Carlo algorithms to investigate two-dimensional multiple-band models, more and more attention is increasingly being devoted to simplified Hamiltonians which make it possible to decrease the number of possible states in the system (t-J-type models[36,60,61]). We believe that this is often unjustified and does not correspond to real experimentally measured parameters of strongly correlated systems such as high-T_c superconductors (see, for example, the parameters of the expanded Hubbard Hamiltonian[62,63]). In addition, the computational results often do not agree with experiment as well as does the multiband Emory model.[64]

In the present paper we present an efficient new trajectory Monte Carlo algorithm for calculating the properties of two-dimensional Cu–O clusters. This method is based on dividing the three-dimensional space-time grid into three-site O–Cu–O cells, and it extends to a two-dimensional grid the corresponding partition presented in Refs. 12–14 for the one-dimensional Hubbard model. In this algorithm the sign problem, which is an obstacle to the development of trajectory methods in two-dimensional fermion systems, has virtually no effect on the convergence because the average sign of the Monte Carlo configuration approaches a constant value. The algorithm makes it possible to calculate the properties of Cu–O clusters with $N_a=24, 30, 48,..., 108,...$ sites with convergence as good as in the standard one-dimensional
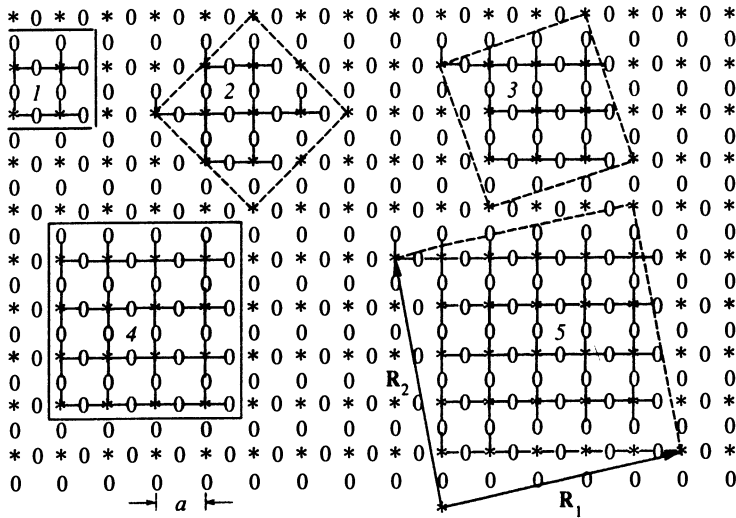
FIG. 1. Square clusters in the CuO_2 plane. *—copper atoms, O—oxygen atoms. The figure shows clusters with N_a sites: $N_a=12$ (1), 24 (2), 30 (3), 48 (4), and 78 (5). Atoms belonging to a cluster are connected by lines.

systems[13] and much better than in standard determinant and variational Monte Carlo methods.[29,46] For this algorithm, the multiband nature of the model considered is unimportant, and as in any trajectory method, the calculation is performed for a canonical ensemble with a fixed total number $\langle N \rangle$ of particles and total spin projection $\langle S_Z \rangle$.

In this paper we consider a sequence of Cu–O clusters with $N_a=12$, 24, 30, 48, 54, 60, 78, 96, 102, and 108 atoms. The clusters possesses square symmetry and admit periodic boundary conditions. The energy, the occupation numbers, the correlation functions, the optical gap in the one-particle spectrum, and the momentum distribution of the carriers are calculated. These properties are determined as functions of the cluster size.

We are aware of numerical results which have now been obtained for Cu–O clusters with $N_a=12$ sites (exact diagonalization method[5-7,10,18]) and $N_a=48$ sites (determinant Monte Carlo method,[35,46] a combination of the determinant Monte Carlo method and molecular dynamics,[38] and the variational Monte Carlo method[65]). Only one author (M. Imada[38]) investigated a cluster with $N_a=108^{1)}$ sites, but he calculated only the occupation numbers and the pair correlation functions. These data are insufficient for determining the dependence of the properties on the cluster size.

The model and the clusters considered are described in Sec. 2. The computational procedure employing the new Monte Carlo trajectory method is described in Sec. 3. The results are presented in Sec. 4.

2. EMORY MODEL AND Cu–O CLUSTERS

The best model for investigating the electronic structure of CuO_2 layers is the two-dimensional multiband Emory model,[4] which takes into account the hybridization of the copper d and oxygen p orbitals, the difference of the atomic levels at the copper and oxygen sites, the Coulomb interaction at the copper and oxygen sites, and the interaction of copper and oxygen sites.

The Emory Hamiltonian in the hole representation is

$$H = -t \sum_{\langle ik \rangle, \sigma} (d_{i\sigma}^+ p_{k\sigma} + \text{h.c.}) + \varepsilon \sum_{k,\sigma} n_{k,\sigma} + U_d \sum_i n_{i\uparrow} n_{i\downarrow}$$

$$+ U_p \sum_k n_{k\uparrow} n_{k\downarrow} + V \sum_{\langle ik \rangle, \sigma, \sigma'} n_{i\sigma} n_{k\sigma'}, \qquad (1)$$

where the operators $d_{i\sigma}^+$ and $p_{k\sigma}^+$ create holes in the $d_{x^2-y^2}$ states and the p_x, p_y states, respectively; $\langle ik \rangle$ indicates summation over nearest neighbors; i and k denote copper and oxygen sites, respectively; $n_{i\sigma}=d_{i\sigma}^+ d_{i\sigma}$ and $n_{k\sigma}=p_{k\sigma}^+ p_{k\sigma}$; t is the copper-oxygen hopping matrix element; $\varepsilon=\varepsilon_p-\varepsilon_d$ is the difference of the hole energies at the oxygen and copper sites; U_d, U_p, and V are the Coulomb repulsion energies of the holes at the copper and oxygen sites and between these sites, respectively. The vacuum for the Hamiltonian (1) is the electronic configuration $Cu3d^{10} O2p^6$ (the valence state of Cu^+O^{2-}). The insulator (undoped) state corresponds to the configuration $Cu^{2+}O^{2-}$ and half-filling with respect to copper (the number of holes $\langle N \rangle$ equals the number of copper sites N_{Cu}).

Next, we partition the CuO_2 plane into clusters which possess the symmetry of an infinite plane (i.e., the symmetry of a square) and therefore admit periodic boundary conditions (see Fig. 1 and Table I). It is convenient to characterize each cluster by the basis vectors R_1 and R_2 (Fig. 1)

$$R_1 = n_x a i + n_y a j, \quad R_2 = -n_y a i + n_x a j, \qquad (2)$$

so that the entire CuO_2 plane is completed covered by these clusters with no superpositions under translations of the form

$$R = p R_1 + q R_2. \qquad (3)$$

In Eqs. (2) and (3) n_x, n_y, p, and q are integers, a is the lattice period (Fig. 1), and i and j are unit vectors along the x and y axes. The correspondence between the cluster sizes and the numbers n_x and n_y is given in Table I. The allowed reciprocal-space vectors for a given cluster are

$$K = (k_x, k_y) = \frac{2\pi}{n_x^2 + n_y^2} (m_1 n_x - m_2 n_y, m_2 n_x + m_1 n_y), \qquad (4)$$

where m_1 and m_2 are integers satisfying the inequalities

TABLE I. Possible square clusters in the CuO_2 plane. Top two numbers—lengths of the sides of a cluster in units of the lattice period a; bottom number—number of sites in a cluster. The product of the upper numbers gives the total number of CuO_2 cells in a cluster. The asterisks (*) mark clusters investigated in the present work.

n_y \ n_x	0	1	2	3	4	5	6	7	8
0		$\sqrt{1}\times\sqrt{1}$ 3	$\sqrt{4}\times\sqrt{4}$* 12	$\sqrt{9}\times\sqrt{9}$ 27	$\sqrt{16}\times\sqrt{16}$* 48	$\sqrt{25}\times\sqrt{25}$ 75	$\sqrt{36}\times\sqrt{36}$* 108	$\sqrt{49}\times\sqrt{49}$ 147	$\sqrt{64}\times\sqrt{64}$ 192
1		$\sqrt{2}\times\sqrt{2}$ 6	$\sqrt{5}\times\sqrt{5}$ 15	$\sqrt{10}\times\sqrt{10}$* 30	$\sqrt{17}\times\sqrt{17}$ 51	$\sqrt{26}\times\sqrt{26}$* 78	$\sqrt{37}\times\sqrt{37}$ 111	$\sqrt{50}\times\sqrt{50}$ 150	$\sqrt{65}\times\sqrt{65}$ 195
2			$\sqrt{8}\times\sqrt{8}$* 24	$\sqrt{13}\times\sqrt{13}$ 39	$\sqrt{20}\times\sqrt{20}$* 60	$\sqrt{29}\times\sqrt{29}$ 87	$\sqrt{40}\times\sqrt{40}$ 120	$\sqrt{53}\times\sqrt{53}$ 159	$\sqrt{68}\times\sqrt{68}$ 204
3				$\sqrt{18}\times\sqrt{18}$* 54	$\sqrt{25}\times\sqrt{25}$ 75	$\sqrt{34}\times\sqrt{34}$* 102	$\sqrt{45}\times\sqrt{45}$ 135	$\sqrt{58}\times\sqrt{58}$ 174	$\sqrt{73}\times\sqrt{73}$ 219
4					$\sqrt{32}\times\sqrt{32}$* 96	$\sqrt{39}\times\sqrt{39}$ 117	$\sqrt{52}\times\sqrt{52}$ 156	$\sqrt{65}\times\sqrt{65}$ 195	$\sqrt{80}\times\sqrt{80}$ 240
5						$\sqrt{50}\times\sqrt{50}$ 150	$\sqrt{61}\times\sqrt{61}$ 183	$\sqrt{74}\times\sqrt{74}$ 222	$\sqrt{89}\times\sqrt{89}$ 267
6							$\sqrt{72}\times\sqrt{72}$ 216	$\sqrt{85}\times\sqrt{85}$ 255	$\sqrt{100}\times\sqrt{100}$ 300
7								$\sqrt{98}\times\sqrt{98}$ 294	$\sqrt{113}\times\sqrt{113}$ 339
8									$\sqrt{128}\times\sqrt{128}$ 384

$$|m_1n_x-m_2n_y|\leqslant(n_x^2+n_y^2)/2,$$

$$|m_2n_x+m_1n_y|\leqslant(n_x^2+n_y^2)/2. \tag{5}$$

For the numerical calculation all clusters with $N_a\leqslant108$ and even N_{Cu} were chosen (indicated in Table I by an asterisk). The requirement that the number of N_{Cu} be even arises because in order to study metal-insulator transitions and to investigate carrier pairing, the situation near half-filling by copper ($\langle N\rangle=N_{Cu}$) is most interesting,[10] and for odd values of N_{Cu} the total projection of the spin $\langle S_z\rangle$ is different from zero, which enhances the finite-size effects. If, however, N_{Cu} is an even number, then we have $\langle S_z\rangle=0$ in the undoped state, just as in an infinite CuO_2 plane.

The obtained sequence of ten clusters with $N_a=12$, 24, 30, 48, 54, 60, 78, 96, 102, and 108 makes it possible to study in detail the effect of the dimension of a system on the electronic properties of the two-dimensional multiple-band Emory model.

3. MONTE CARLO TRAJECTORY METHOD FOR A CuO_2 PLANE

Method for partitioning the space-time grid

The basic idea of any trajectory method is to transform the d-dimensional quantum problem into a $(d+1)$-dimensional classical problem[13] by separating the Hamiltonian into two terms with different types of couplings (even and odd in the one-dimensional case[13,59]):

$$H=H_1+H_2, \quad H_1=\sum_{\langle ij\rangle_1}H_{ij}, \quad H_2=\sum_{\langle ij\rangle_2}H_{ij}. \tag{6}$$

In the case of a CuO_2 plane, we propose the spatial partition illustrated in Fig. 2. The type-1 Cu–O bonds lie to the

right and above the copper atoms and the type-2 bonds lie to the left and below the copper atoms. It is obvious that such a partition divides the entire plane into three-site O–Cu–O cells.

We shall estimate for the partition function

$$Z=Sp[\exp(-\beta H)] \tag{7}$$

the computational error that unavoidably arises with such a partition. We subdivide the interval $[0,\beta]$ into L parts of size $\Delta\tau=\beta/L$. We employ the Trotter expansion[42] in the limits $L\to\infty$ and $\Delta\tau\to0$; specifically, we represent $\exp(-\beta H)$ as the product of exponentials $[\exp(-\Delta\tau H_1)\exp(-\Delta\tau H_2)]^L$. The corrections arising as a result of the noncommutativity of the operators is $\sim(\Delta\tau)^2tA$, where $A=\max(\varepsilon,U_d,U_p,V)$
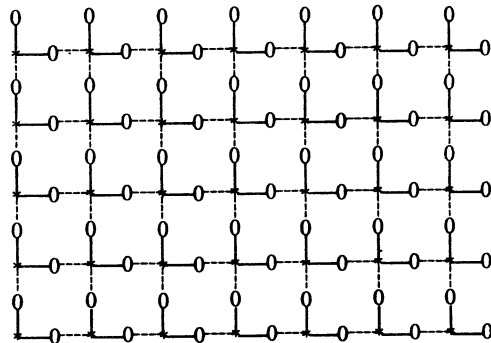

FIG. 2. Partition of the CuO_2 plane into two types of bonds for the Monte Carlo trajectory algorithm (type 1 bonds are marked by solid lines and type 2 bonds are marked by dashed lines).
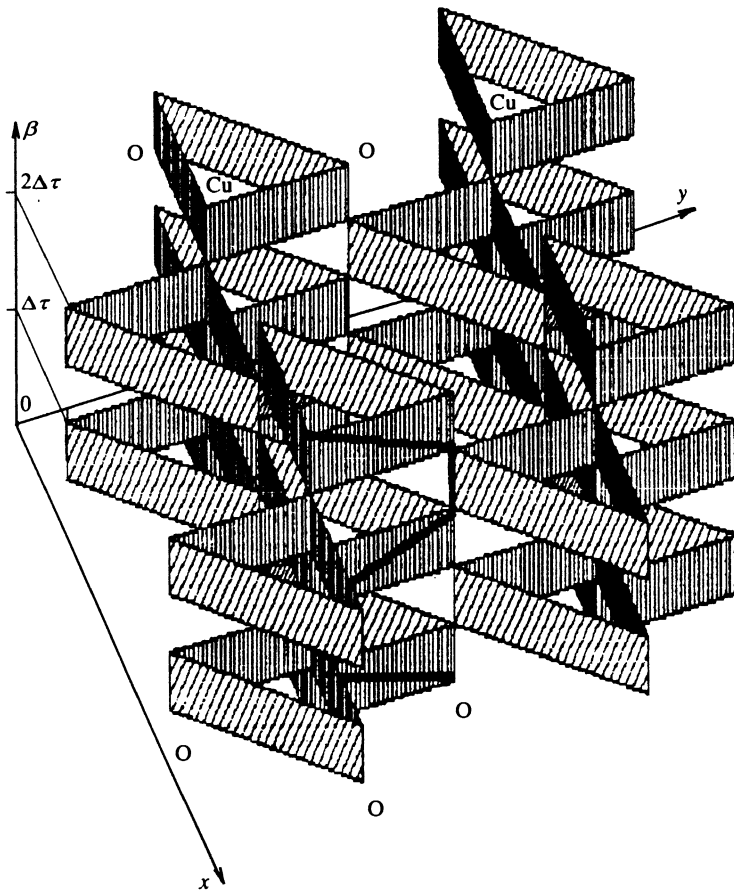
FIG. 3. Space-time grid for the Monte Carlo trajectory algorithm. The fermion world lines can switch only within the vertical hatched faces of the prisms, resting on a O–Cu–O cell.

(see also Ref. 46); in the one-band Hubbard model the error is $\sim(\Delta\tau)^2 tU$ (Ref. 13). In the present work we usually chose $\Delta\tau\sqrt{tA}\leq 0.1$.

Next, inserting in the standard manner a complete system of functions at each time slice, we obtain

$$Z= \sum_{i_1..i_{2L}} \langle i_1|\exp(-\Delta\tau H_1)|i_2\rangle\langle i_2|$$

$$\times\exp(-\Delta\tau H_2)|i_3\rangle.....\langle i_{2L-1}|\exp(-\Delta\tau H_1)|i_{2L}\rangle$$

$$\times\langle i_{2L}|\exp(-\Delta\tau H_2)|i_1\rangle, \tag{8}$$

where

$$|i_m\rangle= \begin{vmatrix} n_{1m\uparrow}n_{2m\uparrow}.....n_{N_a m\uparrow} \\ n_{1m\downarrow}n_{2m\downarrow}.....n_{N_a m\downarrow} \end{vmatrix} \tag{9}$$

and $n_{im\sigma}$ is the occupation number at the site i by holes with spin σ at the mth slice of imaginary time from the interval $[0,\beta]$.

It is convenient to represent the expression (8) graphically. Consider a system of identical two-dimensional Cu–O clusters with N_a atoms, lying one above another along the time axis, the number of such clusters being $2L$ (Fig. 3). The summation in Eq. (8) extends over all possible closed nonintersecting trajectories; the trajectories in the classical lattice obtained can only be switched along the hatched faces of the prisms, resting on the O–Cu–O cells (Fig. 3). To each lattice site there are associated two occupation numbers $n_{m\downarrow}$

and $n_{m\uparrow}$, equal to 0 or 1. For this reason, the trajectories (world lines) occur for each spin independently (the trajectories for different spin projections are independent and influence one another only via the matrix elements of the evolution operator). We note that in each vertical section of the lattice obtained along the Cu–O and O–O lines, the standard two-dimensional checkerboard lattice obtains, typical of the Monte Carlo trajectory method in a system of one-dimensional fermions.[13]

Transitions from one time slice to another are determined by the matrix elements of the evolution operator

$$U_{n,n+1}=\langle i_n|\exp(-\Delta\tau H_{1,2})|i_{n+1}\rangle. \tag{10}$$

The total number of states of a O–Cu–O cell is 64, so that each evolution operator (10) is a 64×64 matrix. The matrix elements for the expression (10) cannot be calculated analytically (unlike spinless-fermion models[13] or the reduced Hubbard model[59] in the one-dimensional situation). To decrease the errors, Eq. (10) was evaluated numerically:

$$U_{n,n+1}=\sum_{L=0}^{\infty} \frac{(-\Delta\tau)^L\langle i_n|H_{1,2}|i_{n+1}\rangle^L}{L!}, \tag{11}$$

where the summation is terminated when the required accuracy is achieved. We note that the expression (11) gives a nonzero probability for switching of a trajectory along the O–O diagonal even in second order in $\Delta\tau$, i.e., a diagonal hop appears (though it did not occur in the initial Hamil-

tonian). For this reason, hole motion along the O–O faces must be taken into account, so that Monte Carlo switching should occur in all three vertical faces of the prisms (hatched in Fig. 3) resting on the O–Cu–O cells.

The summation in Eq. (8) was performed in the standard manner over all admissible closed trajectories. The Metropolis algorithm[44] was used to generate different trajectory configurations. For our problem the algorithm is implemented as follows: The entire lattice of dimension $2(2L \times \sqrt{N_a} \times \sqrt{N_a})$, where the factor of 2 takes into account the spin projections, is scanned, and in each pass over the sites an attempt is made to switch a trajectory without breaking and intersecting another trajectory within the hatched faces of the prism (Fig. 3). The probability of elementary switching of a trajectory is determined by the ratio of the product of the matrix elements (11) before and after switching, and the state of the eight prisms (four per spin projection, Fig. 3), surrounding the prism in which a local trajectory change occurred, is affected (and requires recalculation). In addition, information about the sign of a matrix element (not necessarily positive because the Fermi operators anticommute) may be required to calculate the physical quantities, and for this reason the states of the prisms whose sites are connected by the initial set to the sites affected by the transition can be affected (and subjected to recalculation).

Calculations of thermodynamic averages from the physical quantities

We denote the statistical weight of the kth configuration as

$$W_k = U_{1,2}(k)U_{2,3}(k)....U_{2L,1}(k). \tag{12}$$

Let Q be a diagonal operator in the occupation number representation (for example, $N_{i\sigma} = d_{i\sigma}^+ d_{i\sigma}$ is the number operator for particles with spin projection σ at the ith site). Then, the thermodynamic average of Q over M configurations will have the form

$$\langle Q \rangle = \sum_{k=1}^{M} Q_k P_k, \quad P_k = W_k \bigg/ \sum_{k=1}^{M} W_k, \tag{13}$$

where Q_k is the value of the operator for the kth realization and P_k is the probability of this realization.

As we have already mentioned, the statistical weight W_k is not necessarily positive for two-dimensional fermion models. To calculate the matrix elements, we must keep track of the sign of the wave functions. This makes it necessary each time the trajectory is switched not only the lattice sites which are closest to the region of switching (and whose occupation affects the absolute values of the matrix elements) but also distant sites of the given initial set which are connected with the sites affected by the switching. First, this increases the computational time somewhat and, second, it leads to large statistical errors in Eq. (13) as the temperature decreases. To accelerate convergence of the thermodynamic averages at low temperatures, in this work we employed a somewhat modified expression for the average of an operator, following the procedure of Ref. 58,

TABLE II. Comparison of the data obtained by the Monte Carlo trajectory method, the EDM algorithm (12-site cluster), and the standard Monte Carlo methods (48-site cluster).

Trajectory Monte Carlo method	EDM algorithm ($T=0$)
	$N_a=12 \ \varepsilon=1, \ U_d=6, \ U_p=V=0$
	$\langle N \rangle = 2; \ \langle S_z \rangle = 0$
$E(2)=-3.56\pm0.03, \ T=0.2500$	$E(2)=-4.545512$
$E(2)=-4.08\pm0.04, \ T=0.0625$	
	$\langle N \rangle = 3, \ \langle S_z \rangle = 1/2$
$E(3)=-5.58\pm0.02, \ T=0.1250$	$E(3)=-5.863663$
$E(3)=-5.75\pm0.03, \ T=0.0625$	
	$\langle N \rangle = 4, \ \langle S_z \rangle = 0$
$E(4)=-6.71\pm0.04, \ T=0.2500$	$E(4)=-7.198059$
$E(4)=-7.12\pm0.06, \ T=0.1250$	
$E(4)=-7.15\pm0.06, \ T=0.0625$	
$\langle S_{Cu}S_{Cu}\rangle=0.578\pm0.007, \ T=0.250$	$\langle S_{Cu}S_{Cu}\rangle = 0.546$
$\langle S_{Cu}S_{Cu}\rangle=0.545\pm0.005, \ T=0.250$	
$\langle N_{Cu}\rangle=0.600\pm0.002, \ T=0.250$	$\langle N_{Cu}\rangle=0.569$
$\langle N_{Cu}\rangle=0.574\pm0.002, \ T=0.125$	
$\langle N_O\rangle=0.200\pm0.001, \ T=0.250$	$\langle N_O\rangle=0.216$
$\langle N_O\rangle=0.213\pm0.001, \ T=0.125$	
	$\langle N \rangle = 5, \ \langle S_z \rangle = 1/2$
$E(5)=-7.04\pm0.05, \ T=0.2500$	$E(5)=-7.795229$
$E(5)=-7.70\pm0.09, \ T=0.1250$	
$\langle S_{Cu}S_{Cu}\rangle=0.602\pm0.002, \ T=0.250$	$\langle S_{Cu}S_{Cu}\rangle=0.560$
$\langle S_{Cu}S_{Cu}\rangle=0.577\pm0.002, \ T=0.125$	
$\langle N_{Cu}\rangle=0.664\pm0.002, \ T=0.250$	$\langle N_{Cu}\rangle=0.621$
$\langle N_{Cu}\rangle=0.640\pm0.001, \ T=0.125$	
$\langle N_O\rangle=0.293\pm0.001, \ T=0.250$	$\langle N_O\rangle=0.315$
$\langle N_O\rangle=0.305\pm0.001, \ T=0.125$	
	$\langle N \rangle = 6, \ \langle S_z \rangle = 0$
$E(6)=-7.59\pm0.08, \ T=0.2500$	$E(6)=-8.429312$
$E(6)=-8.40\pm0.08, \ T=0.1250$	
trajectory	Standard
Monte Carlo method	Monte Carlo algorithm from Ref. 35 and 66
	$N_a=48 \ \varepsilon=1.2, \ U_d=6, \ U_p=V=0, \ \langle N \rangle = 16$
$\langle S_{Cu}S_{Cu}\rangle=0.536\pm0.008, \ T=0.125$	$\langle S_{Cu}S_{Cu}\rangle=0.55\pm0.02 \ \varepsilon=1 \ [35]$
$\langle N_{Cu}\rangle=0.561\pm0.003, \ T=0.125$	$\langle N_{Cu}\rangle=0.57\pm0.02 \ \varepsilon=1 \ [35]$
$\langle N_{Cu}\rangle=0.700\pm0.003, \ T=0.15625$	$\langle N_{Cu}\rangle=0.691\pm0.003 \ \varepsilon=2 \ [66]$
$E(16)=-20.58\pm0.22, \ T=0.15635$	$E(16)=20.51\pm0.32 \ \varepsilon=2 \ [66]$

$$P_k = |W_k| \bigg/ \sum_{k=1}^{M} |W_k|,$$

i.e., we neglected the sign of the statistical weight of a configuration. This is valid if the average sign

$$\langle S \rangle = \sum_{k=1}^{M} [(|W_k^+|-|W_k^-|)) \bigg/ \left(\sum_{k=1}^{M} (|W_k^+| + |W_k^-|) \right)$$

approaches a constant value as $\beta \to \infty$.[58] Our calculations confirm this, so that $\langle S \rangle$ approaches a constant value in the limit $T \to 0$.

If the operator Q is not diagonal in the occupation-number representation (for example, the energy $E = -\partial(\ln Z)/\partial\beta$), then the expression (13) becomes somewhat more complicated, and the matrix elements of the form (see, for example, Ref. 13)

TABLE III. Published calculations (including our data) of some properties of ten square Cu–O clusters. Here, * marks data obtained in the present work. The symbol ** in the row for $N_a=12$ indicates that this cluster was investigated in detail by the exact diagonalization method (see, for example, Refs. 5, 7, 10, 17, and 18). We are not aware of any applications of Monte Carlo methods for this cluster (besides the data obtained in the present work). The pair correlation functions (last column) are not applicable to the trajectory Monte Carlo algorithm because of nonlocality.

N_a	$E=\langle H\rangle$	$\dfrac{\langle N_{Cu}\rangle,}{\langle N_O\rangle}$	Δ_{opt}	$\langle S_iS_j\rangle$, $S(\pi\pi)$	$n(k)$	pair correlations
12	[**,*]	[**,*]	[**,*]	[**,]	[**,*]	[**]
24	[*]	[*]	[*]	[*]	[*]	-
30	[*]	[*]	[*]	[*]	[*]	-
48	[46,66] [65,*]	[35,38] [46,48,*]	[65,*]	[35,66,*]	[46,*]	[35,38,46]
54	[*]	[*]	[*]	[*]	[*]	-
60	[*]	[*]	[*]	[*]	[*]	-
78	[*]	[*]	[*]	[*]	[*]	-
96	[*]	-	[*]	-	-	-
102	[*]	-	[*]	-	-	-
108	[38,*]	[66, *]	[*]	[66, *]	[*]	[38, 66]

$$\langle i_n|Q\ \exp(-\Delta\tau H)|i_{n+1}\rangle/U_{n,n+1}$$

must be calculated.

The above discussion referred to operators which conserve the particle number locally. If, however, we are interested in, for example, the momentum distribution function

$$\langle n_\sigma(\mathbf{k})\rangle=\frac{1}{N_{Cu}}\sum_{lm}\langle a_{l\sigma}^+a_{m\sigma}\rangle\exp\{i\mathbf{k}(\mathbf{r}_l-\mathbf{r}_m)\},\qquad(14)$$

then such an operator breaks the fermion world lines, i.e., it does not conserve particle number. Here we have $a_{i\sigma}^+=d_{i\sigma}^+$ if i is a copper node and $a_{i\sigma}^+=p_{i\sigma}^+$ if i is an oxygen node. For example, to calculate the Green's function $G_\sigma(i-j)=\langle a_{i\sigma}^+a_{j\sigma}\rangle$ with nodes i and j that do not belong to the same O–Cu–O cell (nonlocality), additional time slices must be introduced,[13] which slows down convergence considerably. In this work, to calculate $\langle n_\sigma(\mathbf{k})\rangle$ according to Eq. (14) we employed a local approximation, i.e., the sites i and j belong to the same O–Cu–O cell. In this case, the expression (14) is valid for large momenta $(\sim\pi/a)$; nonetheless, this could be sufficient to study the region near a Fermi discontinuity.

To achieve the required accuracy we performed ~2000 Monte Carlo steps for thermalization of the system and ~1000–2000 Monte Carlo steps to calculate the averages. By a Monte Carlo step we mean a single scan of the entire $2(2L\times\sqrt{N_a}\times\sqrt{N_a})$ classical lattice in the Monte Carlo pro-

cedure. The efficiency of this algorithm makes it possible to perform a single measurement $(\sim2000$ Monte Carlo steps) within several hours on a personal computer with a 386 processor.

The statistical errors in the Monte Carlo calculation were estimated by means of the rigorous procedure proposed in Ref. 58:

1) The entire chain of M realizations is divided into N large blocks $(\sim50$–100 Monte Carlo steps per block);

2) the average value Q_j of the given operator over the jth block is calculated;

3) the average and the mean-square deviation are calculated as follows:

$$\langle Q\rangle=\frac{1}{N}\sum_{j=1}^{N}Q_j,\qquad \langle\delta Q\rangle^2=\frac{1}{N-1}\sum_{j=1}^{N}(Q_j-\langle Q\rangle)^2\qquad(15)$$

so that the expected average and the error have the form $\langle Q\rangle\pm\langle\delta Q\rangle/\sqrt{N}$.

To check the algorithm, we compared the computational results both with the data obtained by exact diagonalization of a 12-site Cu_4O_8 cluster and with the data computed by the determinant and variational Monte Carlo method.[35,46,66] The computational results for the energy, the occupation numbers, and some correlation functions of the system are given in Table II.
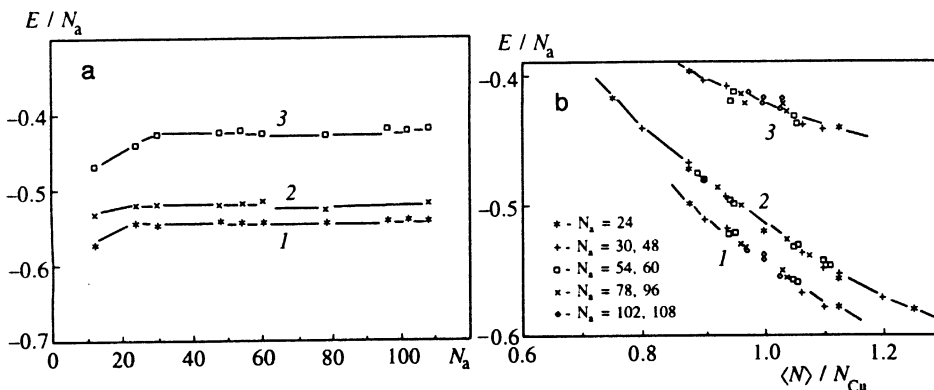

FIG. 4. Average energy per lattice site for square clusters $(U_d=6)$: a) half-filling with respect to copper (undoped state) $\langle N\rangle=\langle N\rangle_{Cu}$. b) Concentration dependence: 1—$\varepsilon=1,\beta=8$; 2—$\varepsilon=1$, $\beta=4$; 3—$\varepsilon=2,\beta=8$.

Legend (panel b):
* - N_a = 24
+ - N_a = 30, 48
○ - N_a = 54, 60
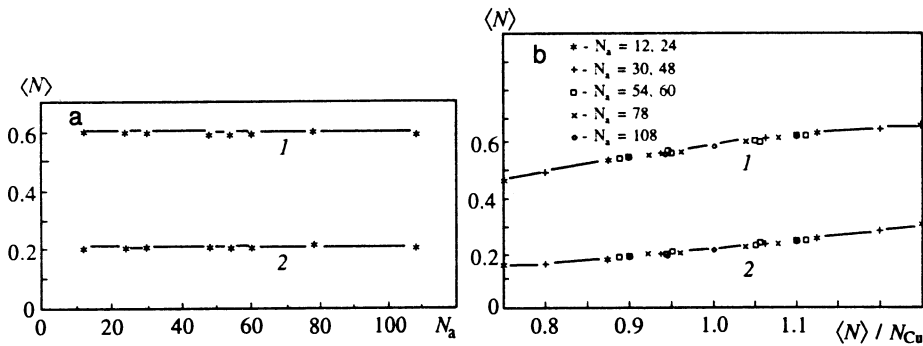× - N_a = 78, 96
• - N_a = 102, 108

FIG. 5. Occupation numbers of copper (1) and oxygen (2) orbitals ($\varepsilon=1$, $U_d=6$, $\beta=4$): a) clusters with $N_a=12$–108; b) effect of doping.

We note that a Cu_4O_8 cluster is extremely small for a Monte Carlo algorithm, which works well when the system contains a quite large number of degrees of freedom. Nonetheless, as one can see from Table II, the results are in good agreement with the exact solution and approach asymptotically the exact solution as $T\rightarrow0$. The larger the number of possible states of the system, the better the convergence (the number of states in a Cu_4O_8 cluster equals 144 for $\langle N\rangle=2$, $\langle S_z\rangle=0$ and 48400 for $\langle N\rangle=6$, $\langle S_z\rangle=0$). In comparing to the Monte Carlo calculations performed using the standard algorithms,[35,66] it is necessary to take into account the fact that the determinant Monte Carlo method employs a large canonical ensemble, i.e., the particle concentration is not fixed but rather is determined by varying the chemical potential. Nonetheless, the results are virtually identical to within the error limits (see Table II); a more detailed comparison to the data obtained by standard Monte Carlo algorithms will be made in Sec. 4. We note that the results agree (to within the indicated errors) with the data of Refs. 46 and 67.

We present below the computational results for the energy of the system, the optical gap, the occupation numbers, the momentum distribution functions, and the spin correlations in different Cu–O clusters nearly half filled with copper.

4. COMPUTATIONAL RESULTS

To facilitate comparisons, Table III gives information about different properties (the energy E, the occupation numbers $\langle N_{Cu}\rangle$ and $\langle N_O\rangle$, the optical gap Δ_{opt}, the spin correlation function $\langle S_iS_j\rangle$ and its Fourier component $S(\pi,\pi)$, the mo-

mentum distribution function $n(\mathbf{k})$, all of which were calculated in the present work as well as previously by other authors. As one can see from the table, the method proposed in the present work makes it possible to obtain a great deal of information about ten clusters (with the exception of pair correlations because of the limitations of the trajectory algorithm), while in the literature available to us only clusters with $N_a=48$ and (for some properties) clusters with $N_a=108$ have been studied in detail. The results obtained in the present work agree, to within the limits of error of the methods, with the data obtained by other authors for clusters with $N_a=48$ and 108. Note that clusters with $N_a=12$, 48, and 108 are special cases, because the unit vectors of the unit cell of these clusters (the basis vectors $\mathbf{R}_1$ and $\mathbf{R}_2$; see Fig. 1) make right angles with the axes of the infinite CuO_2 lattice. The unit vectors of the remaining clusters considered make the angles given in Table I (the tangent of the slope angle equals n_y/n_x). These are the so-called tilted clusters. Of these, the cluster with $N_a=78$ has the smallest tilt angle ($\tan\phi=1/5$). According to the calculations presented below, the characteristics of the system depend not only on the cluster size but also on the values of ϕ.

We calculated the characteristics of the Cu–O clusters in the Emory model for the following values of the parameters: $\varepsilon=1$–3, $U_d=6$, $U_p=V=0$ (in units of t). This choice is determined, first, by the fact that these are typical values of the Emory Hamiltonian, which are calculated on the basis of the experimental data on high-T_c superconductors.[62,63] Second, in this range of values of the parameters the main results for the binding energy of the carriers in a Cu_4O_8 cluster were obtained[10,17,18] by the exact diagonalization method.
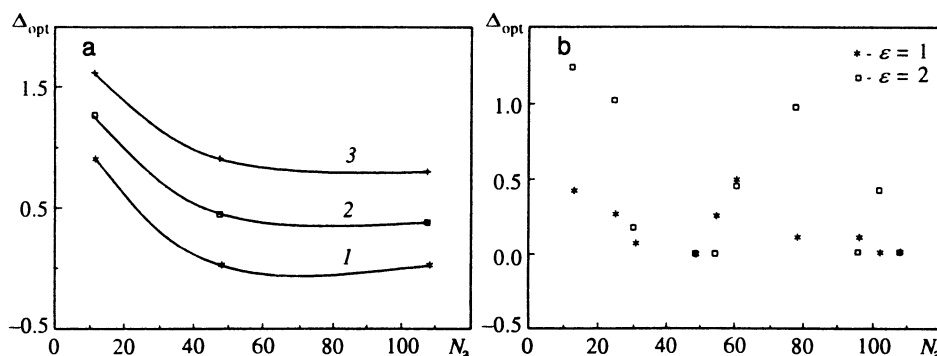

FIG. 6. Optical gap ($U_d=6$, $\beta=8$): a) For $N_a=12$, 48, and 108 for different values of ε: $\varepsilon=2$ (1), 2.5 (2), and 3 (3); b) for clusters with $N_a=12$–108.
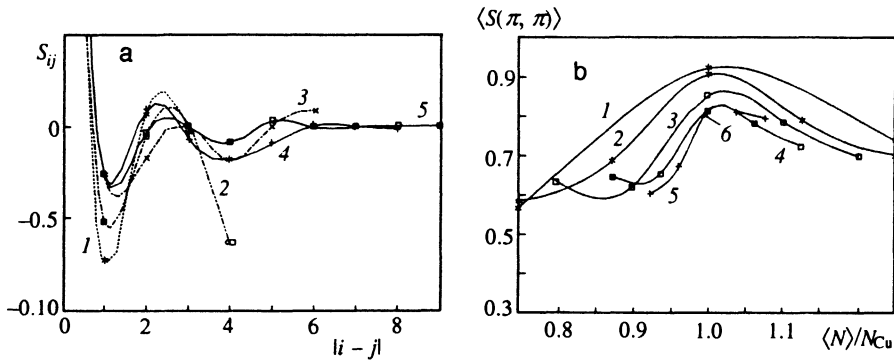
FIG. 7. Spin correlation function on the copper sublattice ($\varepsilon=1$, $U_d=6$, $\beta=4$): a) Dependence on the number of the coordination sphere with respect to copper with half-filling: $N_a=24$ (*1*), 30 (*2*), 54 (*3*), 78 (*4*), and 108 (*5*). b) Effect of doping on the Fourier component with $k=(\pi,\pi)$: $N_a=12$ (*1*), 24 (*2*), 30 (*3*), 48 (*4*), 78 (*5*), and 108 (*6*).

We used the determinant Monte Carlo method[35] to obtain data on the symmetry of the superconducting state in a 48-site Cu–O cluster for close values of the parameters.

Energy and occupation numbers of copper and oxygen orbitals

Figure 4a displays the computational results for the average energy $E=\langle H \rangle$ of the system per lattice site with half filling ($\langle N \rangle = N_{Cu}$) for clusters with $N_a=12$, 24, 30, 48, 54, 60, 78, 96, 102, and 108 sites. One can see that at $N_a=24$ the energy is virtually independent of the cluster size, i.e., it becomes a constant, equal to E in an infinite CuO_2 plane.

Figure 4b displays the energy E as a function of the hole concentration $\langle N \rangle$ in a cluster (the calculations were performed for $\langle N \rangle = N_{Cu}$, $N_{Cu}\pm 1$, and $N_{Cu}\pm 2$). It is obvious that these functions are universal ($\langle N \rangle > N_{Cu}$ for hole doping and $\langle N \rangle < N_{Cu}$ for electron doping).

Figure 5a displays the occupation numbers $\langle N_{Cu} \rangle$ and $\langle N_O \rangle$ in the undoped state versus the size of the system. They are identical for all clusters, including the cluster with $N_a=12$. The universality of $\langle N \rangle$ as a function of the carrier concentration is obvious from Fig. 5b. We emphasize that in the case of hole doping the excess holes occupy predominantly oxygen orbitals, and for electron doping the excess electrons occupy predominantly copper orbitals (in agreement with experiment).

Therefore, characteristics such as E, $\langle N_{Cu} \rangle$, and $\langle N_O \rangle$ do not depend on the cluster size and the tilt angles of the clusters.

Optical gap

The optical gap Δ_{opt} was calculated by the standard formula[65]

$$\Delta_{opt}=E(N_{Cu}+1)+E(N_{Cu}-1)-2E(N_{Cu}) \tag{16}$$

for half-filling with respect to copper; $E(N)$ is the energy of the system with $\langle N \rangle$ holes. The dependence of Δ_{opt} on the cluster (untilted) size for $\varepsilon=2$, 2.5, and 3 is shown in Fig. 6a. One can see that the values of Δ_{opt} approach some asymptotic values. However, as illustrated in Fig. 6b, the results for tilted clusters do not fall on these curves.

We note that our values of Δ_{opt} for $N_a=48$ are identical to the Monte Carlo data obtained by other authors.[65]

Spin correlation functions

The correlation functions

$$S_{ij}=\langle S_{Cu}^z(i)S_{Cu}^z(j) \rangle, \tag{17}$$

defined in the standard manner ($S_{Cu}^z(i) = \langle n_{i\uparrow} - n_{i\downarrow} \rangle$, where i and j are copper sites), were calculated for different degrees of doping and the model parameters $\varepsilon=1$, $U_d=6$, and $\beta=4$. Figure 7a displays S_{ij} as a function of the number of the coordination sphere on the copper sublattice for the undoped state. Note that the number of coordination spheres increases with the cluster size. For this reason, for small clusters the values of $|i-j|$ are bounded by the maximum possible coordination sphere (for $N_a=24$ there are three such spheres, while for $N_a=108$ the number of spheres increases to 12).

Note first the antiferromagnetic character of the correlation functions (the sign of S_{ij} assumes different values as $|i-j|$ increases). Obviously, as the cluster size increases, the amplitude of the antiferromagnetic correlations in the first coordination sphere decreases and saturates at $N_a=78$. The antiferromagnetic correlation length is determined uniquely from Fig. 7a. For clusters with $N_a=78$ and 108 it equals
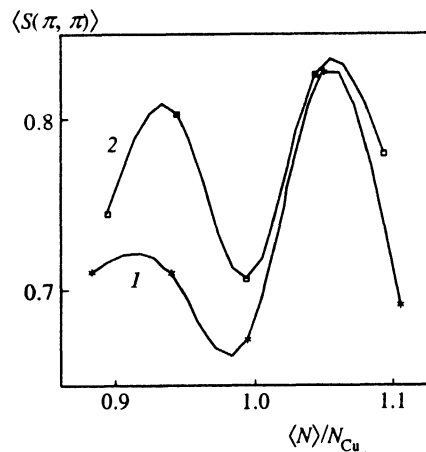

FIG. 8. Fourier component of the spin correlation function on the copper sublattice as a function of doping for strongly tilted clusters with $N_a=54$ (*1*) and 60 (*2*); $\varepsilon=1$, $U_d=6$, and $\beta=4$.
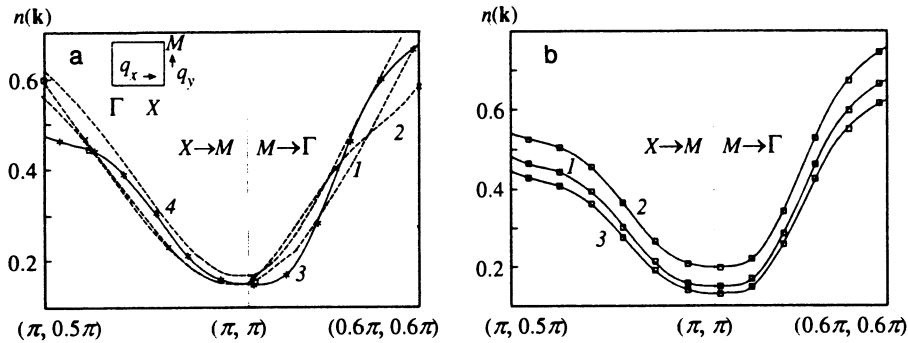
FIG. 9. Momentum distribution function $n(\mathbf{k})$ ($\varepsilon=1$, $U_d=6$, $\beta=4$): a) half filling $\langle N\rangle = N_{Cu}$ near the Fermi jump: $N_a=48$ (1), 60 (2), 78 (3), and 108 (4). b) Effect of doping with $N_a=78$: 1—$\langle N_{Cu}\rangle$; 2—$\langle N_{Cu}\rangle+2$; 3—$\langle N_{Cu}\rangle-2$.

approximately three lattice periods a (six coordination spheres); this is less than the linear size of a cluster (5.1a and 6a, respectively).

Figure 7b displays the Fourier component

$$\langle S(\mathbf{k})\rangle = \frac{1}{N_{Cu}}\sum_{i,j} S_{ij}\,\exp\{i\mathbf{k}(\mathbf{r}_i - \mathbf{r}_j)\} \qquad (18)$$

as a function of the number of holes for different clusters. It is well known that for $\mathbf{k}=(\pi,\pi)$ the correlation function (18) is proportional to the degree of antiferromagnetic ordering on the copper sublattice. It is obvious that the correlation function $S(\pi,\pi)$ decreases with electron and hole doping for practically all clusters (for $N_a=48$ $S(\pi,\pi)$ as a function of $\langle N\rangle/N_{Cu}$ is identical to that calculated in Ref. 35). We note that for strongly tilted clusters with $N_a=54$ and 60 the correlation function behaves differently: doping enhances the initially weak antiferromagnetic correlations (see Fig. 8).

Momentum distribution function of the carriers

The distribution function $n(\mathbf{k})$ was calculated for clusters with $N_a=12$–108 in the local approximation [see Eq. (14)], which is valid for large momenta. The results are displayed in Figs. 9a and 9b for undoped and doped states, respectively. Note that the results for $N_a=48$ are identical to the data given in Ref. 35, where the calculation was performed by the determinant Monte Carlo method without using the local approximation.

Lamentably, the number of allowed values of the momentum for untilted clusters is small (only six per projection for $N_a=108$). For this reason, the results for a cluster with $N_a=78$ are more detailed (14 allowed values of the momenta

per projection). Figure 9a demonstrates quite clearly the displacement of $n(\mathbf{k})$ in the direction of higher energies with hole doping and in the direction of lower energies with electron doping.

Figure 10a displays the functions $n(\mathbf{k})$ for different values of the parameter U_d—the Coulomb repulsion energy at the copper sites. It is obvious that as the interaction becomes stronger, the momentum distribution is displaced downwards and becomes identical to the data of Ref. 35; $n(\mathbf{k})$ practically saturates for $U_d>4$. We also calculated the effect of temperature on $n(\mathbf{k})$. The data (Fig. 10b) show that as the temperature decreases, the spread of $n(\mathbf{k})$ near the Fermi jump decreases. Note also that Figs. 9 and 10 do not show the entire momentum interval. When all momenta are included, the normalization of $n(\mathbf{k})$ ($\sum_{\mathbf{k}\sigma}n_\sigma(\mathbf{k})=\langle N\rangle$) is preserved as U_d and β change.

5. CONCLUSIONS AND RESULTS

The introductory analysis of the existing Monte Carlo algorithms performed together with experience in using the trajectory algorithm proposed in the present work enables us to assess the strengths and weaknesses of these methods:

1. The variational Monte Carlo method depends strongly on the correctness of the initial approximation and is tied to specific models.

2. The determinant Monte Carlo method is free of this drawback, but it is inefficient for multiple-band models.

3. The well-known trajectory algorithms are less sensitive to the multiband nature of the model and they converge more rapidly, but they are employed exclusively for one-dimensional fermion systems.
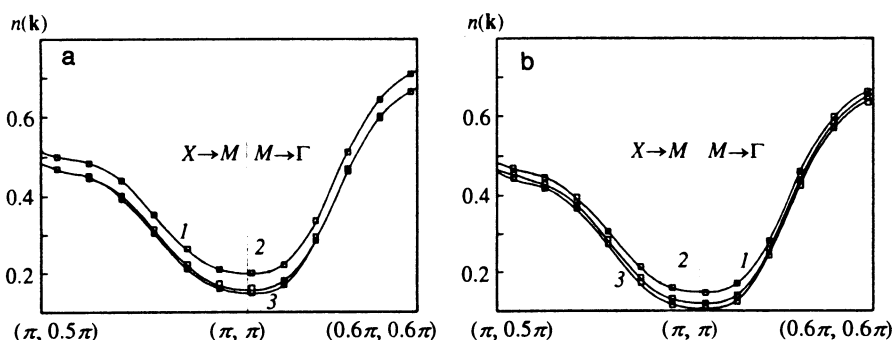

FIG. 10. Momentum distribution $n(\mathbf{k})$ for $N_a=78$ near $\mathbf{k}=(\pi,\pi)$ ($\varepsilon=1$, $U_d=6$, $\beta=4$) as a function of (a) the Coulomb repulsion energy at copper sites $U_d=0$ (1), 4 (2), and 8 (3) and (b) the temperature $\beta=4$ (1), 8 (2), and 16 (3).

4. The algorithm proposed in the present paper (as far as we know, the first trajectory algorithm for a two-dimensional fermion system) also converges rapidly, works well in the case of a multiple-band model, and has no special difficulties with the minus sign problem.

We call attention to several new promising approaches to the numerical modeling of strongly correlated systems. In Ref. 68 a novel method is used to reduce the Hilbert space for the exact diagonalization method in the Lanczos procedure by means of a unique iteration process that selects (according to the parameter t/U) the required site states making the maximum contribution to the ground state. This algorithm can be used to calculate, to good accuracy, the energy of the ground state for a 50-site two-dimensional cluster in the t-J model. In Ref. 69 the variational Monte Carlo method is used in combination with the Lanczos algorithm (EDM). This increases the computational accuracy for the properties of the ground state and avoids the sign problem. Finally, in Ref. 67 the infinite CuO_2 plane is partitioned in the Emory model into clusters with 12 sites, after which each cluster is calculated using the EDM and the results are used to construct a variational function for the ground state of an infinite CuO_2 plane as a superposition of cluster wave functions (an analogous cluster approach is employed in Ref. 70).

In the present paper we have shown for the first time that the energy per lattice site and the occupation numbers become independent of the cluster size at $N_a = 24$, and the amplitudes of the antiferromagnetic (AF) correlations become independent of the cluster size at $N_a = 54$ (for $\beta = 4$). The characteristic attenuation length of AF correlations was determined numerically for the first time, and it was found to be three lattice periods a (i.e., about 1 nm) with a linear cluster size of $5.1a$ ($N_a = 78$) or $6a$ ($N_a = 108$). We note that for high-T_c superconductors, the experimental value of the coherence length in the a-b plane is 1–2 nm.[71] We emphasize that the amplitude of the AF correlations becomes constant (for $N_a = 54$) when the characteristic length of the correlations is approximately equal to the cluster size.

The situation is somewhat more complicated in the case of the optical gap, since Δ_{opt} is sensitive to the tilt angle of the unit cell. In untilted clusters (see Fig. 6a), in contrast to tilted clusters (Fig. 6b), Δ_{opt} approaches a constant value (apparently equal to Δ_{opt} in the infinite CuO_2 plane) as N_a increases.

The results on the effect of doping on $S(\pi,\pi)$, which characterizes the degree of AF ordering (18), are very interesting. According to Fig. 7b, the dependence of $S(\pi,\pi)$ on the degree of doping becomes virtually insensitive to the cluster size at $N_a = 48$ and approaches a universal curve. The rate of suppression of the amplitude of AF correlations decreases with doping. This is an argument in favor of the "magnetic" mechanism for attracting excess carriers (a more detailed discussion is given in Refs. 7–11 and 18).

We call attention to the anomalous behavior of $S(\pi,\pi)$ in strongly tilted clusters with $N_a = 54$ and 60 (see Fig. 8). First, for the undoped state, $S(\pi,\pi)$ is much smaller in strongly tilted clusters than in untilted clusters; this could be associated with the suppression of AF correlations accompanying the tilting of the unit cell. Second, doping increases $S(\pi,\pi)$.

The reasons for these anomalies have not been determined.

Finally, we wish to call attention to the fact that the behavior of the momentum distribution function $n(\mathbf{k})$ in a cluster with $N_a = 78$ (see Figs. 9 and 10) agrees qualitatively with the experimental data obtained by studying positron annihilation in high-T_c bismuth superconductors.[72]

We thank L. A. Openov and A. V. Krasheninnikov for a helpful discussion and a number of valuable remarks, which we used in preparing this paper.

[1)]Some clusters characteristics with $N_a = 108$ are calculated also in Ref. 66.

---

[1] D. C. Mattis, Mod. Phys. Lett. B **4**, 1171 (1990).

[2] F. C. Zhang and T. M. Rice, Phys. Rev. B **37**, 3759 (1988).

[3] G. A. Medina and M. D. Nunez Regueiro, Phys. Rev. B **42**, 8073 (1990).

[4] V. J. Emery, Phys. Rev. Lett. **58**, 2794 (1987).

[5] G. Seibold, E. Sigmund, and V. Hizhnyakov, Phys. Rev. B. **48**, 7537 (1993).

[6] S. Nimkar, D. D. Sarma, H. R. Krishnamurthy, and S. Ramasesha, Phys. Rev. B **48**, 7355 (1993).

[7] J. E. Hirsch, S. Tang, E. Loh Jr., and D. J. Scalapino, Phys. Rev. Lett. **60**, 1668 (1988).

[8] D. Poilblanc, Phys. Rev. B **48**, 3368 (1993).

[9] E. Dagotto and J. Riera, Phys. Rev. Lett. **70**, 682 (1993).

[10] V. F. Elesin, V. A. Kashurnikov, L. A. Openov, and A. I. Podlivaev, Zh. Eksp. Teor. Fiz. **99**, 237 (1991) [Sov. Phys. JETP **72**, 133 (1991)].

[11] K. J. Runge, Phys. Rev. B **45**, 13136 (1992).

[12] J. E. Hirsch, R. L. Sugar, D. J. Scalapino, and R. Blankenbecler, Phys. Rev. Lett. **47**, 1628 (1981).

[13] J. E. Hirsch, R. L. Sugar, D. J. Scalapino, and R. Blankenbecler, Phys. Rev. B **26**, 5033 (1982).

[14] B. Blankenbecler, D. J. Scalapino, and R. L. Sugar, Phys. Rev. B **24**, 2278 (1981).

[15] E. Dagotto, A. Moreo, R. L. Sugar, and D. Toussaint, Phys. Rev. B **41**, 811 (1990).

[16] J. E. Hirsch and R. M. Fye, Phys. Rev. Lett. **56**, 2521 (1986).

[17] V. F. Elesin, V. A. Kashurnikov, and A. I. Podlivaev, Zh. Eksp. Teor. Fiz. **104**, 3835 (1993) [Sov. Phys. JETP **77**, 841 (1993)].

[18] V. F. Elesin, V. A. Kashurnikov, L. A. Openov, and A. I. Podlivaev, Zh. Eksp. Teor. Fiz. **101**, 682 (1992) [Sov. Phys. JETP **74**, 363 (1992)].

[19] E. Dagotto, F. Ortolani, and D. Scalapino, Phys. Rev. B. **46**, 3183 (1992).

[20] A. Moreo, Phys. Rev. B. **45**, 4907 (1992).

[21] H. Eskes and G. A. Sawatzky, Phys. Rev. B. **43**, 119 (1991).

[22] L. Tan, Q. Li, and J. Callaway, Phys. Rev. B **44**, 341 (1991).

[23] V. F. Elesin, V. A. Kashurnikov, A. V. Krasheninnikov, and A. I. Podlivaev, Physica C **222**, 127 (1994); Zh. Eksp. Teor. Fiz. **105**, 1759 (1994) [Sov. Phys. JETP **78**, 951 (1994)].

[24] W. Stefan and P. Horsch, Phys. Rev. B **42**, 8736 (1990).

[25] A. Moreo and E. Dagotto, Phys. Rev. B **42**, 4786 (1990).

[26] D. V. Berkov and S. I. Meshkov, Pis'ma Zh. Eksp. Teor. Fiz. **52**, 1021 (1990) [JETP Lett. **52**, 415 (1990)].

[27] O. Biham, M. Jarell, and C. Jayaprakash, Phys. Rev. B **41**, 2639 (1990).

[28] S. R. White, D. J. Scalapino, R. L. Sugar, and N. E. Bickers, Phys. Rev. Lett. **63**, 1523 (1989).

[29] M. Imada, Physica C **185–187**, 1447 (1991).

[30] S. Sorella, A. Parola, M. Parrinello, and E. Tosatti, Europhys. Lett. **12**, 721 (1990).

[31] R. Valenti and C. Gros, Phys. Rev. Lett. **68**, 2402 (1992).

[32] W. von der Linden, I. Morgenstern, and H. de Raedt, Phys. Rev. B. **41**, 4669 (1990).

[33] H. Aoki and K. Kuroki, Phys. Rev. B **42**, 2125 (1990).

[34] Y. Takada and T. Kita, J. Phys. Soc. Japan **60**, 25 (1991).

[35] R. T. Scalettar, D. J. Scalapino, R. L. Sugar, and S. R. White, Phys. Rev. B **44**, 770 (1991).

[36] M. Imada and Y. Hatsugai, J. Phys. Soc. Japan **58**, 3752 (1989).

[37] H. Otsuka, J. Phys. Soc. Japan **59**, 2916 (1990).

[38] M. Imada, J. Phys. Soc. Japan **57**, 3128 (1988).

[39] H. Yokoyama and H. Shiba, J. Phys. Soc. Japan **56**, 3570 (1987).

[40] Y. Liu, J. Dong, Chang-de Gong, and T. Chen, Phys. Rev. B **48**, 1306 (1993).

[41] H. Yokoyama and H. Shiba, J. Phys. Soc. Japan **59**, 3669 (1990).

[42] M. Suzuki, Phys. Lett. A **113**, 299 (1985).

[43] R. M. Fye, Phys. Rev. B **33**, 6271 (1986).

[44] N. Metropolis, A. W. Rosenbluth, M. N. Rosenbluth *et al.*, J. Chem. Phys. **21**, 1087 (1953).

[45] D. J. Scalapino and R. L. Sugar, Phys. Rev. B **24**, 4295 (1981).

[46] S. J. Sciutto, U. Marini, Bettolo Marconi, and R. Medina, Physica C **171**, 139 (1991).

[47] S. R. White, D. J. Scalapino, R. L. Sugar *et al.*, Phys. Rev. B **40**, 506 (1989).

[48] J. E. Hirsch, Phys. Rev. B **28**, 4059 (1983).

[49] J. E. Hirsch and D. J. Scalapino, Phys. Rev. B **27**, 7169 (1983).

[50] G. G. Batrouni and R. T. Scalettar, Phys. Rev. B **46**, 9051 (1992).

[51] T. Barnes, Int. J. Mod. Phys. C **2**, 659 (1991).

[52] G. G. Batrouni, R. T. Scalettar, and G. T. Zimanyi, Phys. Rev. Lett. **65**, 1765 (1990).

[53] R. T. Scalettar, G. G. Batrouni, and G. T. Zimanyi, Phys. Rev. Lett. **66**, 3144 (1991).

[54] G. G. Batrouni, B. Larson, R. T. Scalettar *et al.*, Phys. Rev. B **48**, 9628 (1993).

[55] G. M. Buendia, Phys. Rev. B **42**, 8163 (1990).

[56] A. Moreo, D. Scalapino, and E. Dagotto, Phys. Rev. B **43**, 11442 (1991).

[57] S. Sorella, S. Baroni, R. Car, and M. Parrinello, Europhys. Lett. **8**, 663 (1989).

[58] N. Furukawa and M. Imada, J. Phys. Soc. Japan **60**, 810 (1991).

[59] S. N. Molotkov, I. A. Ryzhkin, and V. V. Tatarskii, Fiz. Tverd. Tela **31**, 47 (1989) [Sov. Phys. Solid State **31**, 201 (1989)].

[60] F. F. Assaad and D. Wurtz, Phys. Rev. B **44**, 2681 (1991).

[61] T. Barnes and M. D. Kovarik, Preprint ORNL-CCIP-92-03/UTK-92-01, Oak Ridge (1992).

[62] A. K. McMahan, J. F. Annett, and R. M. Martin, Phys. Rev. B **42**, 6268 (1990).

[63] H. Rushan, C. K. Chew, K. K. Phua, and Z. Z. Gan, J. Phys.: Cond. Matt. **3**, 8059 (1991).

[64] A. A. Aligia, Phys. Rev. B **47**, 8929 (1993).

[65] G. Dopf, A. Muramatsu, and W. Hanke, Physica C **185–189**, 1495 (1991).

[66] A. Bhattacharya and C. S. Wang, Phys. Rev. B **48**, 13949 (1993).

[67] T. Wittmann and J. Stolze, Phys. Rev. B **48**, 3479 (1993).

[68] J. Riera and E. Dagotto, Phys. Rev. B **47**, 15346 (1993).

[69] E. S. Heeb and T. M. Rice, Preprint ETH-TH/92-13, Zurich (1992).

[70] A. F. Barabanov, L. A. Maksimov, and G. V. Uimin, Zh. Eksp. Teor. Fiz. **96**, 665 (1989) [Sov. Phys. JETP **69**, 371 (1989)].

[71] Yu. A. Izyumov, Usp. Fiz. Nauk **161**, 1 (1991) [Sov. Phys. Usp. **34**, 935 (1991)].

[72] L. P. Chan, D. P. Harshman, K. G. Lynn *et al.*, Phys. Rev. Lett. **67**, 1350 (1991).

Translated by M. E. Alferieff